Proceedings of the IEEE Dual-Use Technologies & Applications Conference, May 23-26, 1994, V. II, pp. 439-446.

Determination of GPR processing capabilities using ProMAX®

Doria L. Kutrubes
Radar Solutions International, 72 Orange Street, Suite 2, Waltham, MA 02154 *

Jie Zhang, Ph.D.
Randall L. Mackie, Ph.D.
Massachusetts Institute of Technology, Bldg. E-34, 42 Carleton Street, Cambridge, MA 02139

Abstract

A standardized seismic reflection deconvolution algorithm compresses wavelets from reflective horizons and removes unwanted multiples in ideal ground penetrating radar (GPR) data despite inherent differences in GPR wavelet shape. Predictive deconvolution was not effective where lateral velocity changes occur. Processing was also ineffectual where significant GPR signal attenuation occurred because the "constant Q" premise of deconvolution was violated.

I. INTRODUCTION

The dielectric and conductive properties of earth cause frequency-dependent attenuation of EM signals. In one sense, the earth behaves as a filter where the recorded reflected EM energy no longer resembles the idealized earth reflectivity response. Mathematically, the recorded waveform may be expressed as a convolution of the earth's response with the input source wavelet and instrument system response or:

$$x(t) = w(t) * e(t) * n(t) \quad (1)$$

where,

$x(t)$ = the recorded radar trace,
$w(t)$ = the source wavelet
$n(t)$ = the instrument recording response, and
$e(t)$ = the earth's response [1].

The idealized earth's response may be expressed as a reflectivity series (i.e. a series of positive or negative polarity impulse spikes, depending upon the impedance characteristics of the materials at the layered interface). However, source coupling and the ground's propagation characteristics also determine the earth's response. The earth's response may be expressed as a convolution product of the earth reflectivity series with the ground's propagation characteristics and source coupling. The goal of deconvolution, therefore, is to "undo" the filtering effects of the earth and instrument to recover (as closely as possible) the earth's idealized response.

Sheriff [2] defines deconvolution as "the process designed to restore a waveshape to the form it had before it underwent a linear filtering action. On a more pragmatic level, deconvolution processing was developed by the seismic industry to improve the resolution of closely spaced layers (i.e. by recovering the impulse response at each layered interface) and remove unwanted multiples.

Several potential problems may be encountered when using a standard seismic deconvolution wavelet to deconvolve radar data. First, the transmitted radar signal is not similar to its seismic counterpart. The GPR source wavelet approximates a monopulse in air, while the idealized seismic source is an impulse source. Also, the disparity of scales that exists between GPR and seismic wavelets may create difficulties in shaping the deconvolution wavelet as GPR data are generally recorded using a time-window between 50 and 200 nano-seconds (ns) while seismic data are typically recorded in the 1000 to 2000 milliseconds (ms) range. Therefore, the seismic source wavelet may not be a good approximation of its radar counterpart.

To compound this problem, the GPR source wavelet changes frequency, amplitude, and sometimes phase when coupled to the ground, depending upon the dielectric properties of subsurface materials. Differences in seismic and EM wave propagation and attenuation may also be a factor as GPR propagation velocities typically decrease with depth and signal attenuation increases exponentially (and sometimes non-linearly) with depth. Therefore, the "constant Q" premise used in deconvolution may not be valid for GPR data.

Deconvolution also assumes that velocities within any (horizontal) layer remain constant. However, lateral changes in GPR propagation velocity (caused by even slight

* formerly with Geophysical Applications, Inc.

Proceedings of the IEEE Dual-Use Technologies & Applications Conference, May 23-26, 1994, V. II, pp. 439-446.

changes in moisture or clay content, or pore-fluid conductivity) are often significant. Hence, the deconvolved wavelet used in one area may not be a good approximation in another area.

II. DATA INPUT AND PROCESSING

GPR data were collected using 500 MHz and 900 MHz transceiver antennas and the GSSI SIR 10 radar system from five different sites. Raw data, typically recorded as one-channel, non-multiplexed data, was saved on 8mm tape in GSSI 8 bit/512 samples per scan binary format and then transferred to 3 ½ inch floppy drive using the GSSI Radan III software package. Each data file contained between 450 to 2,500 traces. The GPR data were transferred from personal computer to MIT's Unix DEC workstation at the Earth Resources Laboratory. Data were converted to SEG-Y format using a program (OTIS.C) created at Ohio State University and modified for this project.

GPR data sets were deconvolved using the PROMAX® seismic reflection processing package. Data were transferred successfully to ProMAX®, although format differences in the header prevented recording interval (and hence velocity) information from being preserved. Because data were recorded using one transceiver antenna (i.e. one-channel) or two transceiver antennas with different frequencies, a CMP data sort was not necessary and CMP stacking was not possible. A PROMAX® predictive deconvolution algorithm was used to shape the source wavelet.

III. RESULTS

Figure 1 shows raw data from a site in northeast Maine. GPR was used to help characterize materials above a 5 foot depth, and determine the location of shallow bedrock and/or till where blasting and/or excavation may be necessary. Data were recorded for 100 ns. The high-amplitude, continuous reflector which appears midway down on the left and center of Figure 1 (around sample 260 or approximately at 40 to 50 ns) results from reflected GPR energy at the interface between upper (sand) and lower (clay?) layers. Another geologic contact (interpreted as till by GPR and seismic refraction) is observed on the right of Figure 1. Note that deconvolution of this high-quality stratigraphic section is not required to interpret the location and approximate depths of stratigraphic contacts, as typically is the case of about 90 percent of radar data. The goal of using this particular data set, therefore, was to evaluate the performance of predictive deconvolution when an optimum data set is used.

Figure 2 shows deconvolved data from the same site. A prediction lag of 4 (α=4), sample length of 32 (n=32), and pre-whitening factor of 0.001 (ϵ=0.001) produced good results. Note that reflective horizons are significantly compressed and the continuity of the upper reflector is more easily determined.

The second data set was obtained from a Superfund (hazardous waste) Site in New Jersey where the purpose of this survey was to delineate landfill boundaries and buried objects outside these boundaries. Raw data (Figure 3) were recorded for 110 ns using a 500 MHz antenna. Figure 3 shows two dipping reflectors. The reflector located in the center of Figure 3 is the interpreted landfill-natural material boundary. The other dipping reflector is believed to be a compaction layer from within the landfill, created as the landfill was expanded. Note that the interpreted landfill boundary is coincident with a zone of attenuation, best observed at the bottom center and left of Figure 3. The horizontal banding (not true multiples) observed within this area is from instrument noise as all real data has been attenuated. Also, note two hyperbolic reflectors at the right side of Figure 3, which are attributed (and later confirmed) to be drums buried outside of the landfill perimeter. Two or three drums are indicated by the number of hyperbolic reflectors, although interference of waves obscure raw data.

Figure 4 is the show deconvolved section using deconvolution parameters of α=4, n=32, and ϵ=0.001. Note how dipping reflectors are significantly compressed in comparison to the raw data. Also, the predictive deconvolution algorithm was unable to distinguish between real data and noise as the algorithm compressed instrument noise banding. The amplitude of the instrument noise has been reduced; however, this reduction is consistent with the overall reduction in amplitude of the deconvolved section. Predictive deconvolution did not help resolve the number of drums, as anticipated, although the deeper hyperbolic reflector is more difficult to identify because of the reduction in amplitude. Migration was not performed on this data set due to lack of velocity information, although, it would have been the most useful in delineating the number of drums.

The third data set was obtained along a bituminous highway where GPR was used to verify pavement and subbase (capstone underlain by a porous granular material) thicknesses. The raw data, shown on Figure 5 was acquired using a 500 MHz antenna at a 40 ns time-range. The asphalt/capstone boundary (Reflector A) is readily identified in the raw data. Also, two closely-spaced continuous reflectors are identified below the asphalt (corresponding to capstone/granular and granular/clay interfaces or Reflectors B and C, respectively) on the right half of Figure 5.

However, the continuity of the Reflector B is unclear on the other side of the road-seam (left half of Figure 5).

For this example, predictive deconvolution worked best (Figure 6) using a combination of short sample length (n=5), short prediction lag (α=4), and a pre-whitening value of ϵ=0.001. Deconvolution also has improved the resolution between closely-spaced reflectors. A careful inspection of Reflector B indicates that it may be continuous. Also, deconvolution has brought out another reflector (Reflector D) which appears below the interpreted clay reflector.

Figure 7 shows raw data from a similar highway where concrete was used as the highway's pavement instead of asphalt. Data were recorded from a 900 MHz antenna using a 20 ns time window. The concrete-capstone boundary (Reflector A) is not well defined as the contrast in electrical impedance (primarily influenced by dielectric properties) of the two materials is not great. Also, the granular and clay boundary (Reflector C) is poorly defined.

Figure 8 is the deconvolved section of Figure 7 using parameters α=4, n=5, and ϵ=0.001. Resolution of Reflectors A and B has improved, however; Reflector C is still not well defined.

GPR data were obtained from the abutment face of a granite-block bridge to determine its thickness. GPR data were recorded using a 500 MHz antenna and a 100 ns time range. The presence of many undesired reflections make the back of the abutment extremely difficult to identify in the raw data (Figure 9). Multiples are generated from reverberation of GPR signal between the rows of block, while diffractions are created from block edges. Note the dipping reflector (Reflector A) observed between 30 and 40 ns on the left side of Figure 9, which is interpreted as the back of the abutment. The horizontal reflector located at about 45 ns in the central portion of Figure 9 may represent the maximum abutment thickness, although this is a difficult interpretation considering data quality. The goal of deconvolution on this data set was to test the program's effectiveness in removing unwanted multiples and reverberations from poor-quality data.

Figure 10 is the best deconvolved section (n=10 and α=4 and ϵ=0.01). Reflector A has been compressed, but multiples, although minimized, are still present below the dipping reflector. Deconvolution was unable to remove reverberation noise caused by water within the blocks' joints trapping GPR energy. Also, the reflector corresponding to the interpreted back of the abutment has been removed.

IV. CONCLUSIONS

Deconvolution processing using a seismic reflection wavelet is effective on idealized GPR data-sets, which typically do not require any processing to interpret. Results indicate that GPR wavelets can sometimes be approximated by a seismic wavelet. The apparent frequency of reflected GPR signal (and hence the shape of the GPR wavelet) varies with the frequency of the recording antenna, the time-range at which data were recorded, the number of samples per scan, and medium attenuation. All these parameters influence the effectiveness of deconvolution. Long sample lengths (n=32) and short prediction lags (α=4) are best to approximate GPR wavelets from 500 MHz data acquired using a time-range between 100 and 110 ns in low-loss (low conductivity) soil conditions. The sharpest images were generated using a combination of short sample length (n=5) and short prediction lag (α=4) in low-range (25 to 40ns) data.

Deconvolution had minimal or no effect on reflectors where attenuation from conduction losses was great (i.e. not a constant Q). Deconvolution resulted in the compression of the wavelet at the concrete-capstone boundary, for instance, but had little effect on the deeper clay reflector. Deconvolution was also ineffective in removing unwanted, high-frequency reverberations. Future research may include obtaining multi-offset data which can be used for velocity analysis, stacking (i.e. increasing the signal to noise ratio), and the removal of multiples. Migration may also be useful in removing diffractions from data and determining the number of discrete targets (such as drums).

V. REFERENCES

[1] O. Yilmaz, "Seismic data processing," Society of exploration geophysicists, Tulsa, OK, 1987, p.96.

[2] R.E. Sheriff, "Encyclopedic dictionary of exploration geophysics," Society of Exploration Geophysicists, Tulsa, Oklahoma, 1973, p. 47.

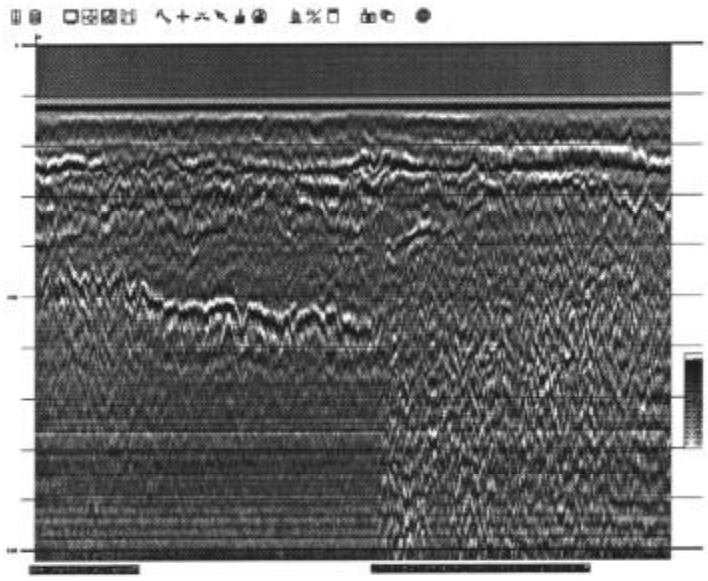

Figure 1: GPR record from a site in northeast Maine. Data were collected at 100 ns using a 500 MHz antenna. Note geologic contact on right side of figure.

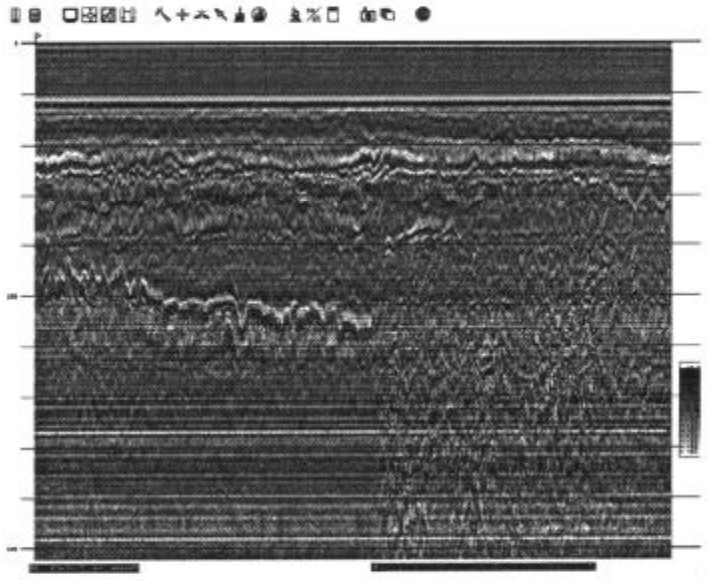

Figure 2: Deconvolve section from same site using $\alpha = 4$, $n = 32$, and $\epsilon = 0.001$.

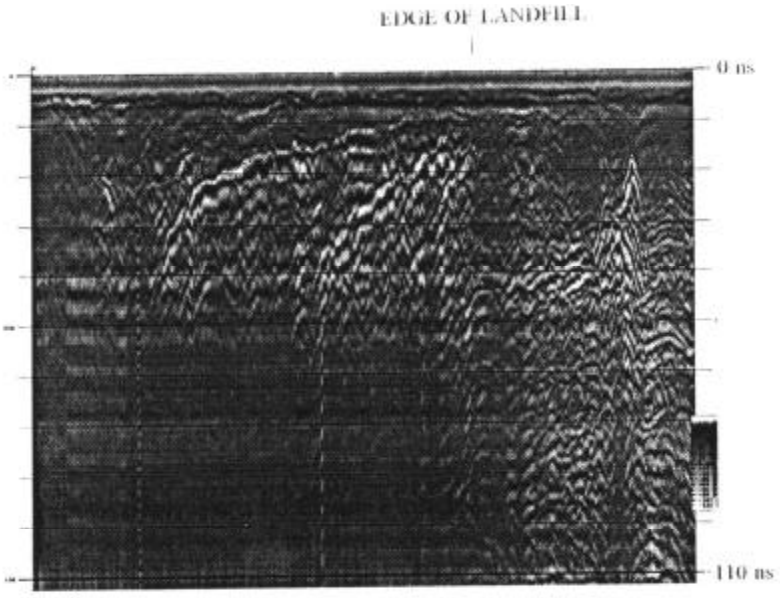

Figure 3: GPR record from a Superfund (landfill) site in New Jersey. Data were collected at 110 ns using a 500 MHz antenna. Note approximate landfill boundary denoted by zone of attenuation (bottom) and dipping reflector in center of figure, interpreted as the landfill/ natural soil boundary. Also note hyperbolic reflectors outside of landfill which are attributed to buried drums.

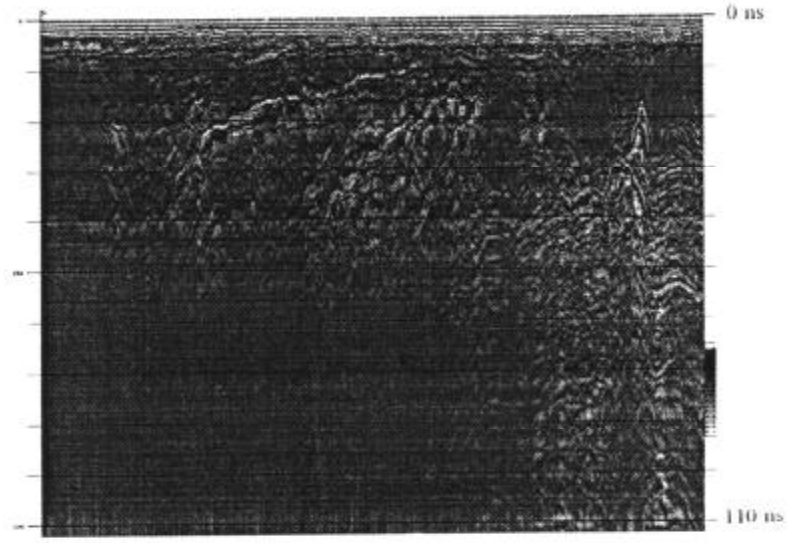

Figure 4: Deconvolved section from same site using $\alpha = 4$, $n = 32$, and $\epsilon = 0.001$.

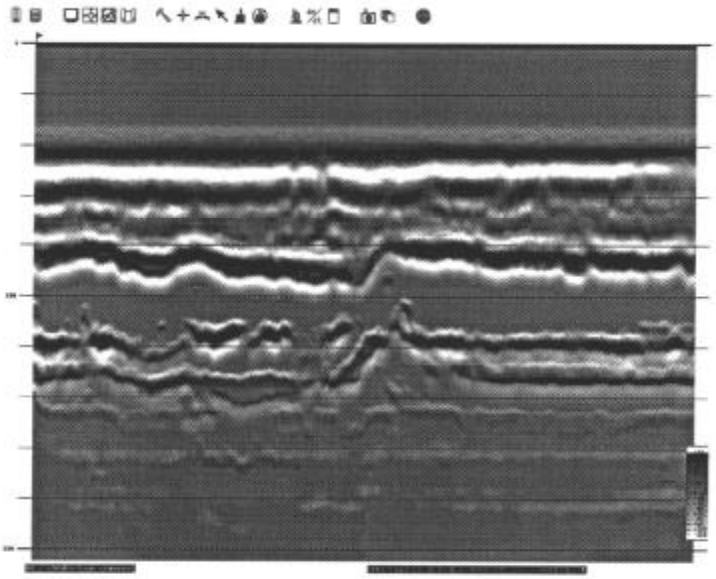

Figure 5: GPR record from a highway in Illinois. Data were collected at 40 ns using a 500 MHz antenna. Note the road seam location at the center of the record. The upper reflector is the asphalt/subbase interface. Subbase reflectors appear discontinous to the left of the road seam.

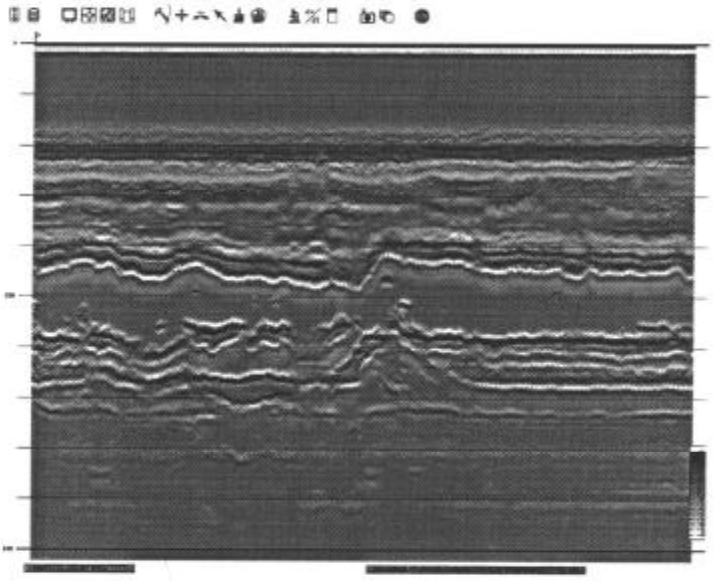

Figure 6: Deconvolved section from same site using $\alpha = 4$, $n = 5$, and $\epsilon = 0.001$.

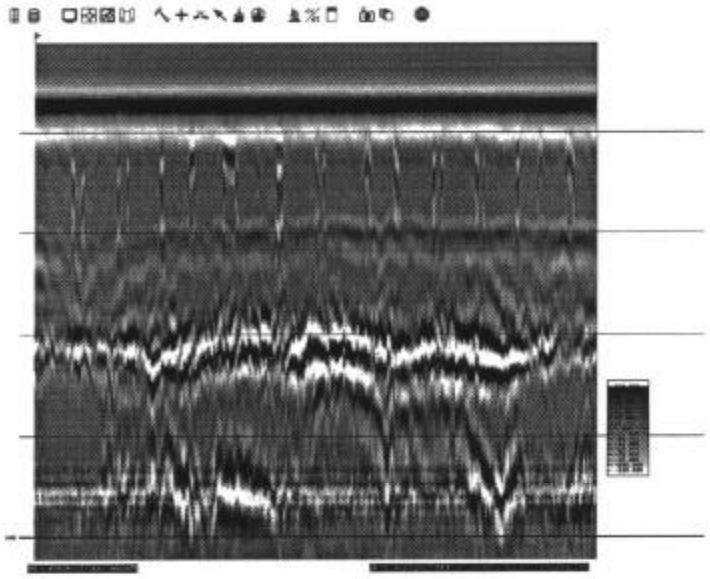

Figure 7: GPR record from a concrete highway. Data were collected at 25 ns using a 900 MHz antenna. Note upper reflector delineates the concrete/subbase boundary while middle reflector denote a change in subbase composition. The weak bottom reflector marks the subbase/clay boundary.

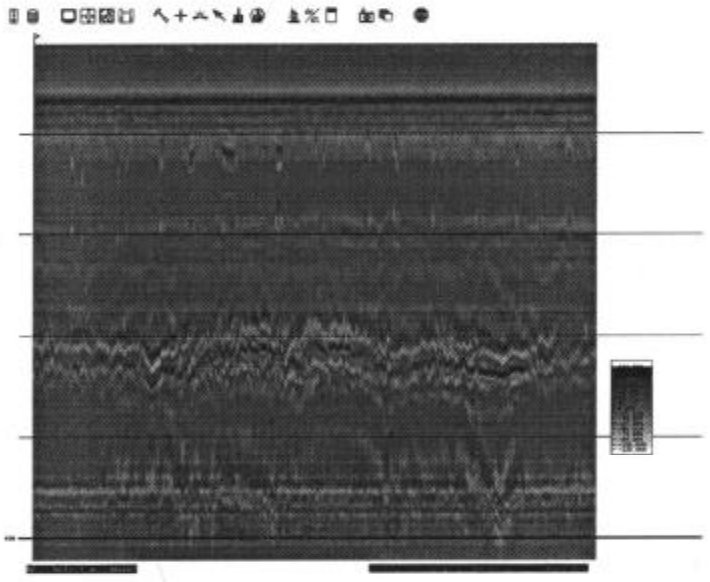

Figure 8: Deconvolved section from same site using $\alpha = 4$, $n = 5$, and $\epsilon = 0.001$.

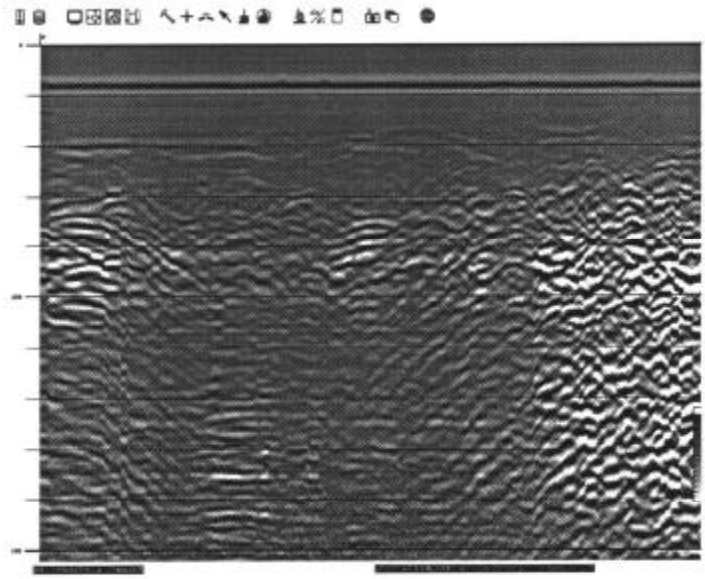

Figure 9: GPR record from a granite-block abutment. Data were collected at 100 ns using a 500 MHz antenna. The antenna was towed across the abutment's face. Note the dipping reflector on the left, interpreted as the abutment/fill contact. The weak reflector located at about 45 ns (center) corresponds to the abutment/fill contact at the abutment's thickest point. Water within blocks' joints make it imposible to observe the abutment/fill contact on the right.

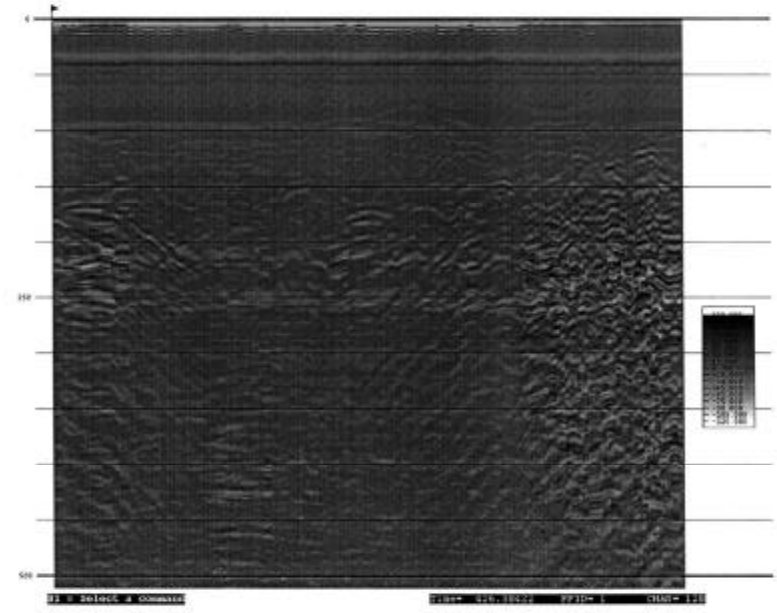

Figure 10: Deconvolved section from same site using $\alpha = 4$, $n = 10$, and $\epsilon = 0.01$.